Available online at www.sciencedirect.com
ScienceDirect
Journal of the European Ceramic Society 30 (2010) 1203–1209
www.elsevier.com/locate/jeurceramsoc

# $ZrO_2$ ceramics with aligned pore structure by EPD and their characterisation by X-ray computed tomography

Kirsten Moritz [a,*], Tassilo Moritz [b]

[a] Technische Universität Bergakademie Freiberg, Institute of Electronic and Sensor Materials, Gustav-Zeuner-Str. 3, 09596 Freiberg, Germany
[b] Fraunhofer Institute for Ceramic Technologies and Systems, Winterbergstr. 28, 01277 Dresden, Germany

Available online 23 June 2009

**Abstract**

Using the electrolytic gas generation during the electrophoretic deposition (EPD) from aqueous suspensions, planar zirconia green bodies with unidirectionally aligned pore channels were produced. Number, diameter distribution, and arrangement of the pore channels could be controlled by the experimental conditions such as the electrolyte content of the suspension, the applied electric field strength, and the kind of the deposition electrode. The green bodies were sintered at 1450 °C in air. Besides optical microscopy and mercury porosimetry, X-ray computed tomography was used for characterising the porous samples. The CT investigations were well suited for this purpose because they enabled a three-dimensional characterisation of the pore structure by a non-destructive method.


*Keywords:* Electrophoretic deposition; Non-destructive evaluation

## 1. Introduction

The electrophoretic deposition is usually aimed at the production of green bodies or layers with dense particle packing. Therefore, the electrolysis of water leading to the formation of hydrogen at the cathode and of oxygen at the anode is undesirable in the majority of cases. Non-aqueous suspensions are often used for the EPD to avoid the electrolytic gas evolution. Because of the advantages of water-based EPD regarding environment, health, and costs, different methods have been developed to prevent large pores caused by gas generation when using aqueous suspensions. The simplest way is the EPD below the decomposition voltage of water, but it is only practicable for thin layers by reason of the low deposition rate.

A successful approach is the membrane method. The deposit is formed at a membrane positioned in front of the deposition electrode, not at the electrode.[1]

In case of the deposition at the cathode, electrode materials which absorb hydrogen (e.g., palladium) were used to produce bubble-free deposits.[2,3]

In anodic deposition, the oxygen evolution can be prevented using easily oxidisable anodes such as zinc.[4–6] Drawback of this method is the contamination of the deposit with metal cations originating from the anodic oxidation of the electrode. Another possibility is the addition of an electrolyte which is oxidised. Electrolytes showing at least two valences such as bromides or iodides are suitable for this purpose.[1] Additions of hydroquinone were also successfully used.[7]

Recent publications describe that the gas bubble formation during the electrophoretic deposition from aqueous suspensions can be avoided when a pulsed-DC field of suitable pulse width[8] or an asymmetric AC field[9] is applied instead of the commonly used continuous DC field.

Only a few investigations are known which take advantage of the electrolysis of water during EPD to produce porous ceramics. The method was first used by Kerkar[10] for the fabrication of ceramic bodies having conically shaped pores which ranges from 0.5 μm to 5 μm in diameter at the narrow end and from 20 μm to 200 μm at the wide end (wall thickness of the ceramic body: 1–5 mm). The production of alumina and zirconia tubes, respectively, with conical pores in radial direction was taken as an example. A graphite rod served as deposition electrode. Furthermore, the EPD into a graphite crucible was described. The graphite electrodes were burned out during sintering in air.

The production of tubular ceramic bodies with unidirectionally aligned pore channels by the same electrophoretic method

* Corresponding author at: Technische Universität Bergakademie Freiberg, Institute of Electronic and Sensor Materials, Gustav-Zeuner-Str. 3, 09596 Freiberg, Germany. Tel.: +49 3731 392077; fax: +49 3731 393662.
*E-mail address:* kirsten.moritz@esm.tu-freiberg.de (K. Moritz).

0955-2219/$ – see front matter © 2009 Elsevier Ltd. All rights reserved.
doi:10.1016/j.jeurceramsoc.2009.05.034

is also the topic of two further publications.[11,12] In a similar manner as described by Kerkar,[10] graphite rods were used as deposition electrodes. The pore structure was influenced by the pH value and the current. Starch was added to increase the porosity of the ceramics.[12] The porous bodies were characterised by optical and SEM micrographs.

In the present paper, the fabrication of planar $ZrO_2$ bodies with aligned pore structure by electrophoretic deposition and simultaneous electrolytic gas bubble formation will be described.

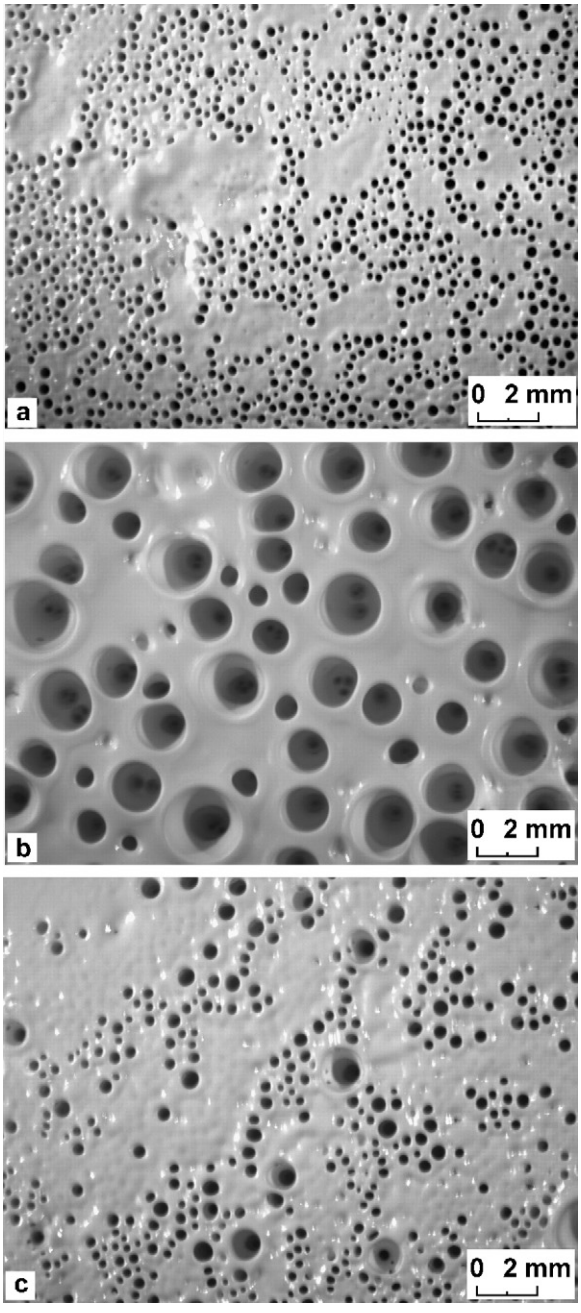


Fig. 1. Optical micrographs of green body surfaces showing the influence of the applied voltage and of the electrolyte content on the pore structure (EPD on platinum foil). (a) $1.8 \times 10^{-3}$ ml glacial acetic acid/g powder; 5 V, 60 min. (b) $1.8 \times 10^{-3}$ ml glacial acetic acid/g powder; 30 V, 20 min. (c) $0.9 \times 10^{-3}$ ml glacial acetic acid/g powder; 30 V, 20 min.

The pore structure can be controlled by several parameters such as the kind and amount of electrolytes and other additives (e.g., dispersants, surfactants, binding agents), the solid content of the suspension, the electrical parameters of the EPD (voltage, current), the kind of the deposition electrode, and the electrode separation. By way of example, the influence of the electrolyte content, of the applied voltage, and of the structure of the deposition electrode (foil with smooth surface compared with gauze) will be shown.

X-ray computed tomography as a non-destructive testing method has been used for characterising the porous structures. For X-ray computed tomography, the sample is positioned between the X-ray source and the detector and rotates by an angle of 360°. Using a flat panel detector, the total volume of the sample can be captured with a single rotation. The cross-sections of the sample are calculated by a reconstruction algorithm using the result of the radiation images. By means of visual display software, inhomogeneities or defects in the sample can be made visible.[13–15] In our case, a three-dimensional characterisation of the pore structures was the purpose of the CT investigations.

## 2. Experimental procedure

The zirconia powder TZ-3Y from Tosoh/Japan ($Y_2O_3$ content: 5.22 wt%, specific surface area: 14.8 $m^2$/g, crystallite size: 280 Å) was used as starting material. It was dispersed in deionized water, and the suspensions were ultrasonicated for 3 min by means of an ultrasonic horn (Sonopuls HD 2200, Bandelin, Germany). The solid content of the suspensions was 40 wt%. Already without any additives, the zeta potential and suspension stability were adequate for a successful electrophoretic deposition as described in a former publication,[16] but glacial acetic acid (100%, Merck, Germany) was added to the suspension for promoting the electrolytic gas generation. In order to ensure sufficiently high electrophoretic mobility and suspension stability, electrokinetic measurements and sedimentation tests had been carried out in preliminary investigations. In both cases, without

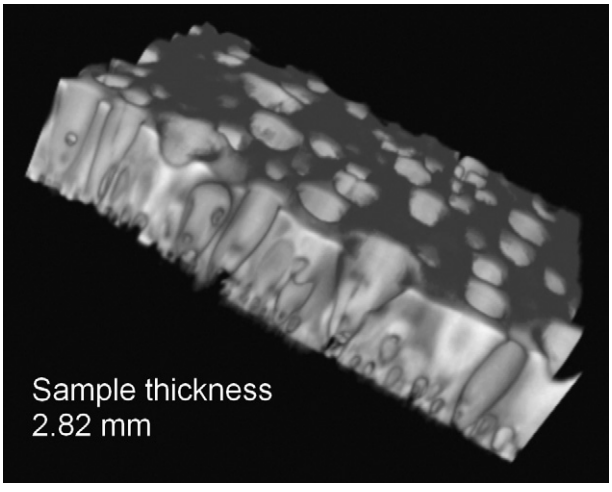


Fig. 2. Image section of the CT 3D-reconstruction of the sample shown in Fig. 1b (CT investigation after sintering).

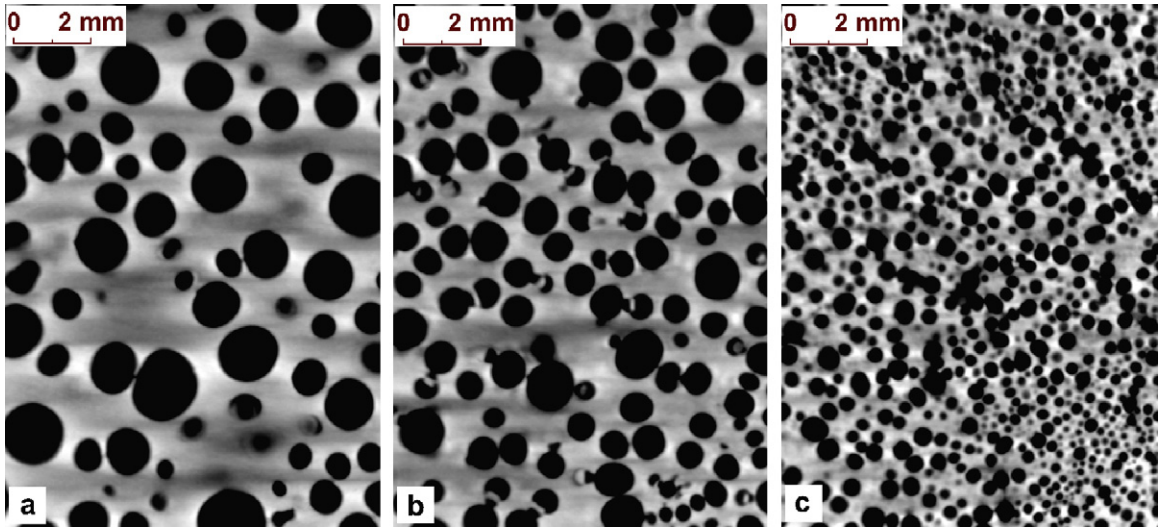


Fig. 3. Cross-sections of the CT 3D-reconstruction shown in Fig. 2. (a) 0.45 mm from top side. (b) Middle. (c) 0.45 mm from bottom side. (Thickness of the sintered body: 2.82 mm.)

additives and with acetic acid, the surfaces of the particles were positively charged.

The specific electrical conductivity was measured by means of the conductometer LF 92 (wtw, Germany).

Rectangular planar green bodies with dimensions of 25 mm × 20 mm were produced by constant-voltage EPD in the direction of the gravitational force. Typical thicknesses of the deposits were in the range between 2 mm and 4 mm. Platinum foil and platinum gauze (225 meshes/cm$^2$, wire diameter: 0.12 mm) positioned on platinum foil, respectively, were used as deposition electrode. A platinum foil with the same dimensions (25 mm × 20 mm) served as opposite electrode. The electrodes were separated by a distance of 20 mm.

The porous green bodies were warily removed from the electrode, dried at ambient temperature and sintered at 1450 °C/2 h holding time in air.

For characterising the pore structure of the green and sintered bodies, optical microscopy (stereomicroscope "Technival", JENOPTIC Jena, Germany) and X-ray *c*omputed *t*omography were used. The CT investigations were carried out using the tomograph "CT-Compact" made by PROCON X-Ray/Germany and the Fraunhofer Development Centre X-Ray Technique Fürth/Germany. It is a 3D-X-ray device equipped with a 150 kV microfocus radiator with a radiation power of 75 W and 750 mm distance between focal spot and detector. The flat panel detector allows a resolution down to 21 μm. The electrophoretically deposited samples were investigated at 130 kV and a radiation power of 26 W.

By image analysis (a4i IMESa, Soft Imaging System, Germany), the pore diameter distributions in different levels of the 3D-reconstructions obtained by the CT investigations were determined.

In addition, a selected green body was characterised by mercury porosimetry. Pore diameters from 5 nm to 500 μm can be measured by the used porosimeter (AutoPore IV 9500, Micromeritics). Thus, this method is suitable to characterise the interparticular porosity in the skeleton of the porous green bodies. The pore channels formed by electrolysis can be detected provided that their diameters are within the measuring range. Furthermore, they should not show a pronounced conicity because in mercury porosimetry cylindrical pores are assumed for determining the pore sizes. Considering these criteria, a green body with relatively fine pore channels was chosen for this investigation. The particle packing in the skeleton of the porous sample was compared with a "dense" deposit from the same suspension produced by EPD using the membrane method (see Section 1). For the electrophoretic deposition according to the membrane method, an EPD cell consisting of two compartments separated by a dialysis membrane made of regenerated cellulose was used. The suspension was poured in one compartment. The other one contained a solution of acetic acid with a specific electrical conductivity of 1.2 mS/cm. The distance between electrode and membrane in the suspension chamber was 4 cm. In the electrolyte chamber, the other electrode was

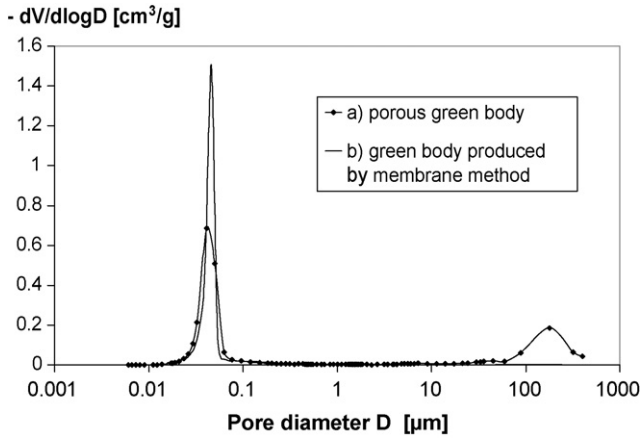


Fig. 4. Pore diameter distributions determined by mercury intrusion. Curve (a) porous green body produced under the following conditions: $1.8 \times 10^{-3}$ ml glacial acetic acid/g powder; EPD on platinum foil at 15 V, 45 min. Curve (b) green body produced by the membrane method (EPD conditions: see "Section 2").

separated from the membrane by a distance of 2 cm. A constant voltage of 40 V was applied for 15 min. Since the particles were deposited at the membrane, the green body contained no pores formed by gas bubbles.

## 3. Results and discussion

Fig. 1a compared with Fig. 1b shows the strong influence of the applied voltage on the resulting pore structure. A higher voltage at the same electrode distance, i.e., higher field strength, leads not only to an increase in deposition rate but also to an increased intensity of gas bubble formation because, according to Faraday's first law of electrolysis, the quantities of substances involved in the chemical change are proportional to the quantity of electricity passing through the electrolyte.[17]

Small pore diameters were obtained at a low applied voltage of 5 V and an electrolyte content of $1.8 \times 10^{-3}$ ml glacial acetic acid/g $ZrO_2$ (Fig. 1a). Some of the pores were covered with a thin solid layer arising from suspension wetting the sample surface. Though no open ends are visible in some areas of the sample surface, also these areas contain fine pore channels. The thickness of the deposit shown in Fig. 1a is 2.07 mm. Because of the low field strength, an unusually long deposition time of 60 min was chosen for producing this sample.

By contrast, the EPD at an applied voltage of 30 V led to a deposit with large pores. On the bottom of these pores smaller ones in the first layer of the deposit can be seen (Fig. 1b). At this increased voltage, a sample thickness of 3.70 mm was obtained in a deposition time of 20 min.

The same EPD conditions (30 V, 20 min) but only the half amount of acetic acid ($0.9 \times 10^{-3}$ ml glacial acetic acid/g $ZrO_2$) were used for producing the green body shown in Fig. 1c. The specific electrical conductivity of the suspension was 0.448 mS/cm instead of 0.629 mS/cm. Due to the reduced gas generation at the lower electrolyte content, the resulting pore diameters were significantly smaller compared with the sample in Fig. 1b. In comparison with the deposit in Fig. 1a, however, the micrograph of the sample surface indicates a broader pore diameter distribution. Similar to the sample in Fig. 1a, a thin solid layer covers some of the pores. The thickness of the green body is 3.61 mm.

Due to the high stability of the used suspensions against particle agglomeration, a dense, homogeneous particle packing in the skeleton of the porous bodies was obtained which provided sufficient mechanical stability for green bodies handling.

Results of the CT investigation of the deposit shown in Fig. 1b can be seen in Figs. 2 and 3 (CT investigation after sintering). As illustrated by the image section of the 3D-reconstruction in Fig. 2 and by the cross-sections in Fig. 3, many small pores were formed at the beginning of the EPD. In the further course of the deposition, the pores were growing and merging. At the electrolyte content and the voltage used in case of this sample, large pore diameters were obtained on the top side, but there were also pore channels which did not reach the sample surface. By image analysis of Fig. 3a (i.e., 0.45 mm from the top side of the sample), a mean pore diameter of 813 μm was measured.

In the following example, a green body with a finer pore structure has been characterised by mercury porosimetry in addition to computed tomography. Curve "a" in Fig. 4 shows the pore diameter distribution determined by mercury intrusion. The peak at approximately 40 nm can be attributed to the pores between the particles in the skeleton. It is consistent with the pore size distribution of the green body deposited from the same suspension by the membrane method (curve "b") and indicates a dense and homogeneous particle packing. The second peak at large pore diameters reflects the pore channels formed by electrolytic gas generation.

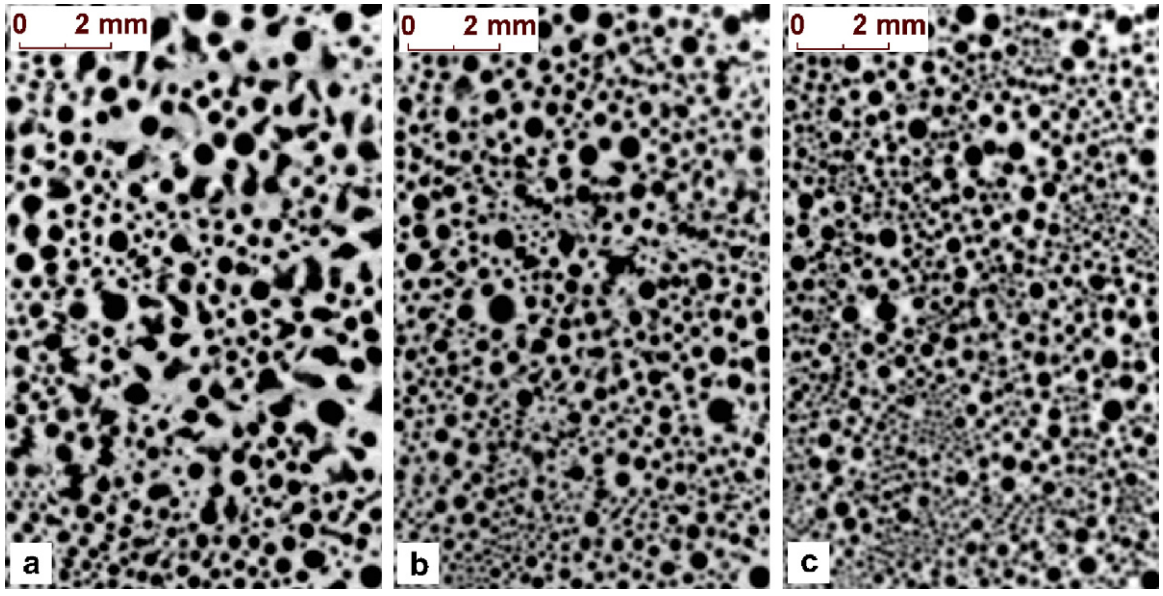


Fig. 5. Cross-sections obtained by computed tomography of a green body deposited under the following conditions: $1.8 \times 10^{-3}$ ml glacial acetic acid/g powder; EPD on platinum foil at 15 V, 45 min (same sample as in Fig. 4, curve "a"). (a) 0.5 mm from top side. (b) Middle. (c) 0.5 mm from bottom side. (Thickness of the green body: 3.4 mm.)

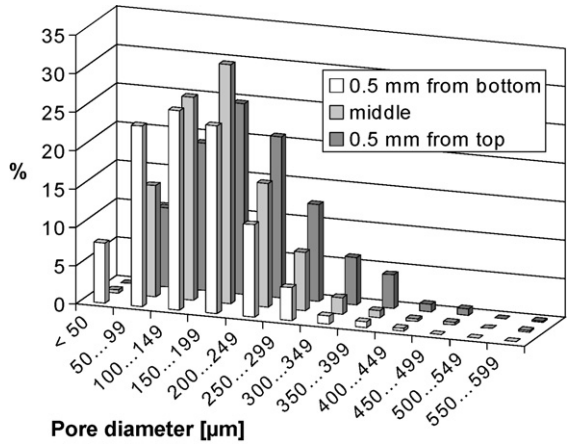


Fig. 6. Pore diameter distributions determined by image analysis of the cross-sections shown in Fig. 5.

Cross-sections obtained by CT investigation of the same porous green body are shown in Fig. 5. The pore size distributions in these cross-sections determined by image analysis can be seen in Fig. 6. In the section plane at a distance of 0.5 mm from bottom side, 74% of the pores are within the range $50\,\mu m \leq d < 200\,\mu m$. The maximum of the distribution is at $100\,\mu m \leq d < 150\,\mu m$. In the middle regarding the sample thickness, the pore size distribution shows a shift in the direction of larger pores. In this cross-section, the maximum is located at pore diameters ranging from 150 µm to <200 µm. At a distance of 0.5 mm from the top side, the position of the maximum has not changed, but it is lower in favour of an increased percentage of larger pores.

Despite the different measuring principles, mercury porosity and analysis of CT images led to similar results concerning the diameters of the pore channels formed by gas bubbles. Image analysis allowed a more precise determination of the pore diameters in the range of these large pores. A further advantage was the possibility to measure the pore sizes in different cross-sections. For characterising the particle packing in the skeleton, mercury porosimetry was well suited. The interparticular pores could not be detected by computed tomography because the resolution was too low. In mercury intrusion, the number of measuring points in the range of large pores (negative pressure region) is small (see Fig. 4) leading to a reduced accuracy. Thus, both methods complement one another.

Fig. 7 compares optical micrographs of the surface of green bodies produced under identical EPD conditions but using different deposition electrodes. The thicknesses of the deposits were determined to be 2.91 mm (sample in Fig. 7a) and 3.02 mm (sam-

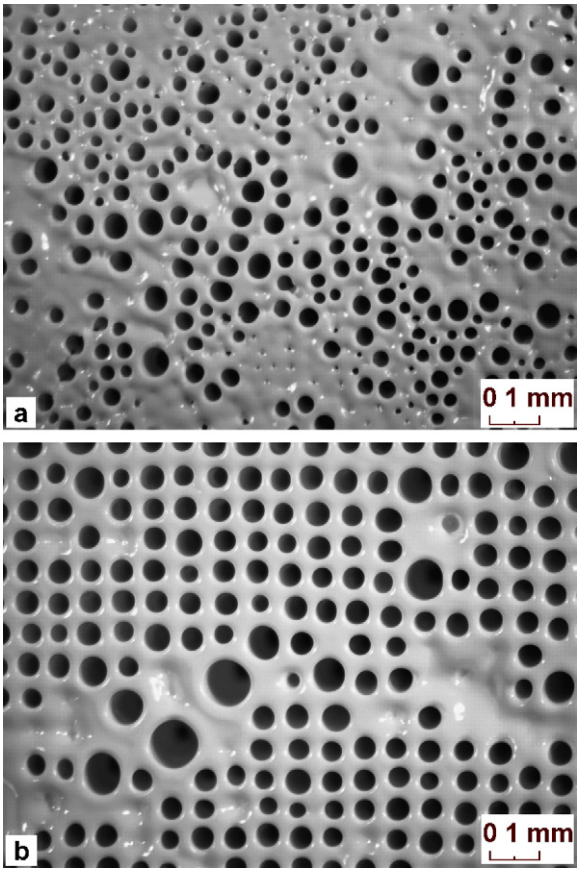


Fig. 7. Optical micrographs of green body surfaces showing the influence of the deposition electrode; $1.8 \times 10^{-3}$ ml glacial acetic acid/g powder; 10 V, 60 min. (a) EPD on platinum foil. (b) EPD on platinum gauze positioned on platinum foil.

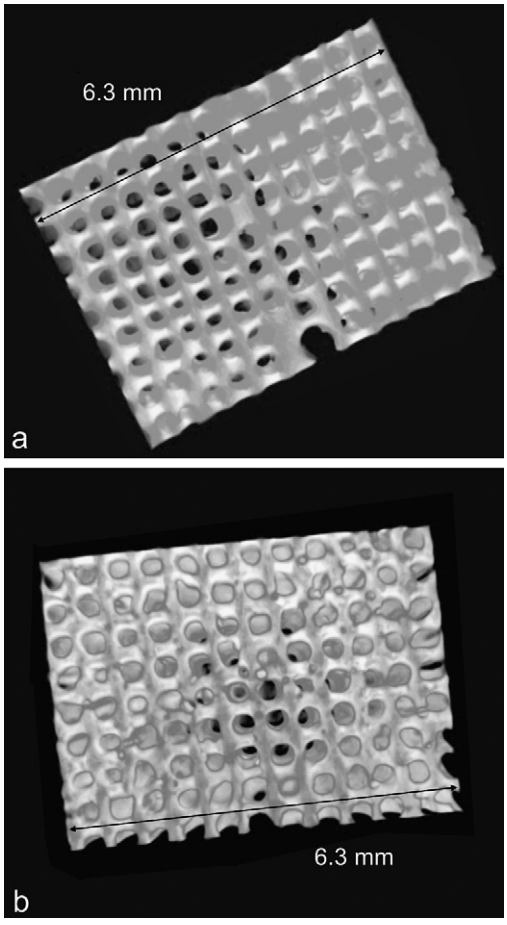


Fig. 8. Image section of the CT 3D-reconstruction of the sample shown in Fig. 7b (CT investigation after sintering). (a) Top side. (b) Bottom side. (Thickness of the sintered body: 2.4 mm.)

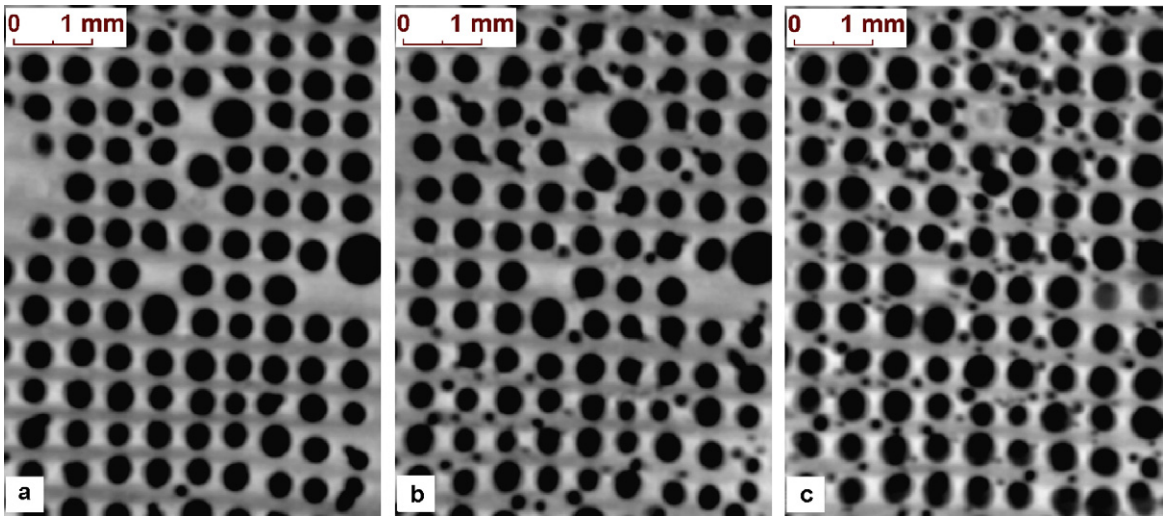


Fig. 9. Cross-sections of the CT 3D-reconstruction shown in Fig. 8. (a) 0.55 mm from top side. (b) Middle. (c) 0.55 mm from bottom side. (Thickness of the sintered body: 2.4 mm.)

ple in Fig. 7b), respectively. In contrast to the random distribution of the pores obtained by EPD on platinum foil (Fig. 7a), the EPD on platinum gauze positioned on the foil resulted in a very regular pore arrangement. Only a few greater pores were out of this regular arrangement (Fig. 7b). The pore channels were formed over the meshes of the gauze, not over the crossed wires.

After sintering, the deposit shown in Fig. 7b was also investigated by computed tomography. Fig. 8 shows an image section of the 3D-reconstruction of the sintered sample (Fig. 8a: top view and b: bottom view). Selected cross-sections of the CT reconstruction can be seen in Fig. 9. In addition to the regularly arranged pore channels formed over the meshes, small pores are visible in the section plane near the bottom side (Fig. 9c). The number of small pores decreases with increasing distance from the lower side (Fig. 9b). There are hardly any small pores near the top side (Fig. 9a).

The pore diameter distributions in these three cross-sections were determined by image analysis (Fig. 10). At a distance of 0.55 mm from bottom side, i.e., in the section plane shown in Fig. 9c, the pore diameters show a bimodal distribution with maxima in the ranges $50\,\mu m \leq d < 100\,\mu m$ and $300\,\mu m \leq d < 350\,\mu m$. In the middle regarding the sample thickness (cross-section in Fig. 9b), the maximum at small pores is lower. Accordingly, the percentage of the pore diameters in the range of the second maximum ($300\,\mu m \leq d < 350\,\mu m$) which can be attributed to the pore channels formed over the meshes is higher. Near the top side (cross-section in Fig. 9a), the pore size distribution shows a further increase in this second maximum. The percentage of small pores can be neglected.

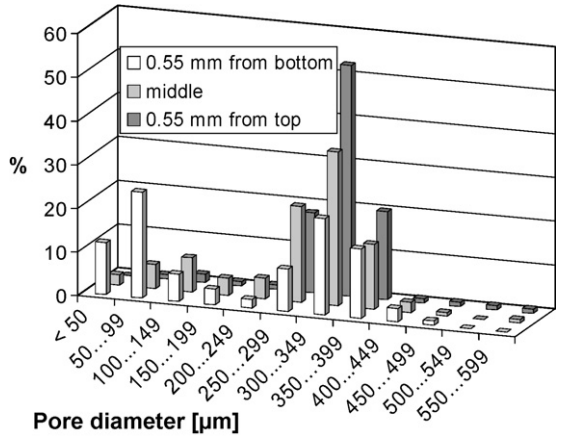


Fig. 10. Pore diameter distributions determined by image analysis of the cross-sections shown in Fig. 9.

## 4. Summary

Electrophoretic deposition from aqueous suspensions with simultaneous gas bubble formation by electrolysis is a suitable method for fabricating ceramics with unidirectionally aligned pore channels. Planar porous $ZrO_2$ green bodies were produced by this method. For promoting the gas generation, glacial acetic acid was added to the suspension. The acetic acid concentration, the applied voltage, and the kind of deposition electrode strongly influenced the resulting pore structure. Whereas the use of platinum as deposition electrode led to a random arrangement of the pore channels, deposits with very regularly arranged pores could be obtained by EPD on platinum gauze positioned on the foil.

X-ray computed tomography allowed a 3D-reconstruction of the porous structures by a non-destructive characterisation method.

## Acknowledgement

Financial support by the Deutsche Forschungsgemeinschaft is gratefully acknowledged.

## References

1. Clasen, R., Forming compacts of submicron silica particles by electrophoretic deposition. In *Ceramic Powder Processing Science*, ed. H.

Hausner, G. L. Messing and S. Hirano. DKG, Köln, 1989, pp. 633–640.
2. Uchikoshi, T., Ozawa, K., Hatton, B. D. and Sakka, Y., Dense, bubble-free deposits from aqueous suspensions by electrophoretic deposition. *J. Mater. Res.*, 2001, **16**(2), 321–324.
3. Tang, F. Q., Uchikoshi, T., Ozawa, K. and Sakka, Y., Electrophoretic deposition of aqueous nano-γ-$Al_2O_3$ suspensions. *Mater. Res. Bull.*, 2002, **37**(4), 653–660.
4. Chronberg, M. S. and Händle, F., Processes and equipment for the production of materials by electrophoresis ELEPHANT. *Interceram*, 1978, **27**(1), 33–34.
5. Ferrari, B., Farinas, J. C. and Moreno, R., Determination and control of metallic impurities in alumina deposits obtained by aqueous electrophoretic deposition. *J. Am. Ceram. Soc.*, 2001, **84**(4), 733–739.
6. Tang, F. Q., Sakka, Y. and Uchikoshi, T., Electrophoretic deposition of aqueous nano-sized zinc oxide suspensions on a zinc electrode. *Mater. Res. Bull.*, 2003, **38**(2), 207–212.
7. Sakurada, O., Suzuki, K., Miura, T. and Hashiba, M., Bubble-free electrophoretic deposition of aqueous zirconia suspensions with hydroquinone. *J. Mater. Sci.*, 2004, **39**(5), 1845–1847.
8. Besra, L., Uchikoshi, T., Suzuki, T. S. and Sakka, Y., Bubble-free aqueous electrophoretic deposition (EPD) by pulse-potential application. *J. Am. Ceram. Soc.*, 2008, **91**(10), 3154–3159.
9. Neirinck, B., Fransaer, J., Van der Biest, O. and Vleugels, J., Aqueous electrophoretic deposition in asymmetric AC electric fields (AC-EPD). *Electrochem. Commun.*, 2009, **11**, 57–60.
10. Kerkar, A. V., Manufacture of conical pore ceramics by electrophoretic deposition. US Patent 5 472 583, 1995; EP 0589 548 A1, 1994.
11. Nakahira, A., Nishimura, F., Kato, S., Iwata, M. and Takeda, S., Green fabrication of porous ceramics using an aqueous electrophoretic deposition process. *J. Am. Ceram. Soc.*, 2003, **86**(7), 1230–1232.
12. Nakahira, A., Ishihara, S. and Nakamura, S., Syntheses and evaluation of porous ceramics by electrophoretic deposition method. *J. Ceram. Soc. Jpn.*, 2007, **115**(6), 383–387.
13. Maisl, M. and Netzelmann, U., Rapid Testing muss Rapid Manufacturing ergänzen – Stoffliche Defekte und Gefüge rasch, zuverlässig und kostengünstig zerstörungsfrei prüfen – auch bei Stückzahl eins. [Rapid Testing must complete Rapid Prototyping – quick, reliable and inexpensive non-destructive testing of material defects and microstructures – even at lot size one]. In *Proceedings of Euro-u Rapid 2006, International User's Conference on Rapid Prototyping & Rapid Tooling & Rapid Manufacturing*, ed. R. Meyer, 2006, pp. 1–6.
14. Wolter, K. J., Daniel, D. and Danczak, M., Röntgen-Computertomografie zur Qualitätssicherung in der AVT. [X-ray computed tomography for quality ensurance in assembling and joining technology]. *GMM-Fachbericht*, *vol. 44*. VDE-Verlag, Berlin, Offenbach, 2004, pp. 227–231.
15. Pfeifer-Schäller, I. and Klein, F., Zerstörungsfreie Bauteilprüfung an Aluminium- und Magnesium-Druckgussteilen mithilfe der Computertomografie. [Non-destructive testing of aluminium and magnesium pressure die castings with 3-dimensional computer tomography]. *Giesserei-Rundschau*, 2003, **50**(5/6), 109–116.
16. Moritz, K., Thauer, R. and Müller, E., Electrophoretic deposition of nanoscaled zirconia powders prepared by laser evaporation. *cfi/Ber. DKG*, 2000, **77**(8), E8–E14.
17. Bagotsky, V. S., *Fundamentals of Electrochemistry* (*2nd ed.*). John Wiley Sons, Hoboken, NJ, 2006, p. 15.